Hippocampal Theta-Gamma Coupling Reflects State-Dependent Information Processing in Decision Making

Seiichiro Amemiya[1] and **A. David Redish**[1,2,*]

[1]Department of Neuroscience, University of Minnesota, Minneapolis, MN 55455, USA

SUMMARY

During decision making, hippocampal activity encodes information sometimes about present and sometimes about potential future plans. The mechanisms underlying this transition remain unknown. Building on the evidence that gamma oscillations at different frequencies (low gamma [LG], 30–55 Hz; high gamma [HG], 60–90 Hz; and epsilon, 100–140 Hz) reflect inputs from different circuits, we identified how changes in those frequencies reflect different information-processing states. Using a unique noradrenergic manipulation by clonidine, which shifted both neural representations and gamma states, we found that future representations depended on gamma components. These changes were identifiable on each cycle of theta as asymmetries in the theta cycle, which arose from changes within the ratio of LG and HG power and the underlying phases of those gamma rhythms within the theta cycle. These changes in asymmetry of the theta cycle reflected changes in representations of present and future on each theta cycle.

In Brief

*Correspondence: redish@umn.edu.
[2]Lead Contact
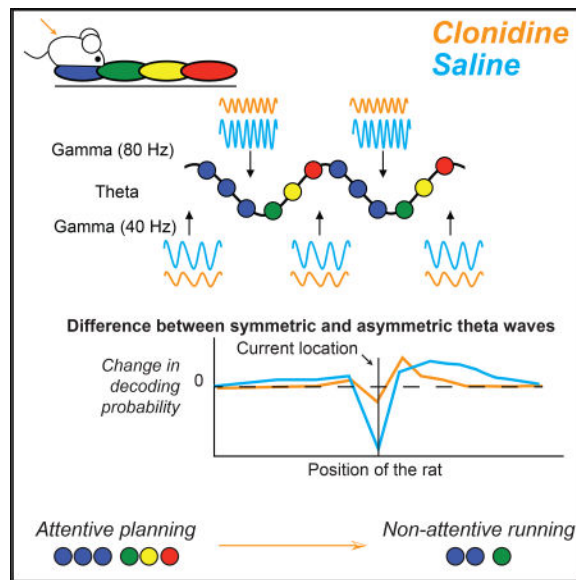
Amemiya and Redish find that hippocampal spatial representation from current to future locations depends on a balance of low gamma (30–55 Hz) and high gamma (60–90 Hz) oscillations within each theta cycle and disrupt this balance through a noradrenergic clonidine manipulation, which reduces future representations.

INTRODUCTION

The hippocampus plays a central role in episodic memory (Cohen and Eichenbaum, 1993), navigation (O'Keefe and Nadel, 1978; Redish, 1999), planning (Hassabis and Maguire, 2007; Redish, 2016; Spiers and Maguire, 2006), and episodic future thinking (Schacter et al., 2007). All of these processes depend on the ability to simulate spatially and temporarily remote information, whether to remember the past or to imagine the future. Simulation processes re-use the same neural systems as perception (Johnson and Redish, 2007; O'Craven and Kanwisher, 2000; Pearson et al., 2015; Redish, 2016). This means that within any experimental task, some hippocampal cell activities reflect current signals about the immediate present and some cell activities reflect non-local cognitive processing.

Hippocampal cells in rodents fire spikes at specific locations within the environment (the place field of each place cell) (O'Keefe and Dostrovsky, 1971). Following the previous logic of perception and simulation, some place cell spikes represent the current location of the animal, while other place cell spikes represent plans or memories. An example of this can be seen in individual place fields, in which a portion of the field (typically the end of the field) represents the actual location of the rat but a separate portion of the field reflects a representation of the potential future path of the animal (Lisman and Redish, 2009). This planning process can also be seen in the theta sequences that occur during attentive behaviors in the rat. During attentive behaviors, the local field potential shows a 6–12 Hz theta rhythm (O'Keefe and Nadel, 1978; Vanderwolf, 1971). During each cycle of theta, the hippocampal place cells fire in order of their place fields along the path of the rat in the direction of travel (Foster and Wilson, 2007; Maurer and McNaughton, 2007). These two

descriptions are duals of each other: when rats are planning paths to a goal, the sequence goes farther to the goal and the place fields begin earlier in the journey (Wikenheiser and Redish, 2015).

The mechanisms underlying this transition from present to future in these sequences remains unknown, but it may be possible to access these processes through different interactions with gamma oscillations. Gamma oscillations (30–140 Hz) interact with theta to temporally organize the activity of place cell populations (Lisman and Redish, 2009). The gamma oscillations split into distinct components reflecting different information processing in CA1 from different origins, including a low-frequency component (30–55 Hz, arising from interactions with CA3), a high-frequency component (60–90 Hz, arising from interactions with entorhinal cortex), and a higher component, termed epsilon (100–140 Hz, arising from intra-CA1 circuits) (Belluscio et al., 2012; Colgin et al., 2009; Lasztóczi and Klausberger, 2016; Sullivan et al., 2011).

When rats face difficult decisions, they sometimes pause and re-orient toward paths, a behavioral process termed vicarious trial and error (VTE). During VTE, at decision points, the population of place cells sweeps forward ahead of the rat toward potential paths in each theta cycle (Johnson and Redish, 2007), akin to the within-theta sequences seen during normal navigation along a path (Foster and Wilson, 2007; Gupta et al., 2012). These sequences go farther ahead than typical theta sequences (Johnson and Redish, 2007; Papale et al., 2016). During VTE, different fundamental frequencies within the gamma range become transiently active, aligned with decision times (Takahashi et al., 2014; Yamamoto et al., 2014), suggesting that gamma oscillations modulate the transition of representation from present to future.

In previous studies, we found that systemic clonidine, an α2 noradrenergic auto-receptor agonist, which decreases tonic noradrenaline levels (Saunier et al., 1993), behaviorally and mentally suppressed VTE processes—both the behavioral manifestation of VTE and the forward representations in hippocampus within theta cycles (Amemiya et al., 2014; Amemiya and Redish, 2016). In this study, we analyze changes in the underlying hippocampal neural mechanisms under this unique clonidine manipulation to elucidate the mechanisms by which hippocampus differentiates representations of the immediate present from the non-local processes.

RESULTS

We recorded neural activity from the CA1 region of hippocampus from 4 rats (Fisher-Brown Norway hybrids [FBNF-1]) as they ran a spatial decision-making task in a modified Hebb-Williams maze (Figure 1A). Rats learned to run through a changeable central path (the navigation sequence [NS]), turning left or right for food at the choice point (CP). If the rat made the correct choice, it received two food pellets at the side feeder (Fs) and two more at the center feeder (Fc). On a subset of days, systemic clonidine (30 μg/kg) or saline vehicle was delivered intraperitoneally 30 min before the session (30 saline sessions and 30 clonidine sessions were analyzed).

Rats sometimes showed vicarious trial and error (VTE) behaviors at the choice point of the maze (Figure 1B). VTE was objectively quantified with zIdPhi, a measure of the Z-scored integrated absolute angular velocity over the choice point pass (Papale et al., 2012). Consistent with previous studies, we defined laps with zIdPhi > 0.5 as VTE laps. As already reported, clonidine suppressed, but did not eliminate, VTE events on this task (Amemiya and Redish, 2016). zIdPhi was higher in VTE laps than in non-VTE laps (n = 30, $p < 10^{-6}$ for saline; n = 30, $p < 10^{-6}$ for clonidine; rank-sum test, two sided) (Figure 1C). On trials that showed VTE, the amount of head movement was not different between drug conditions (p = 0.3, rank-sum test, two sided) (Figure 1C). Running speed was slower on VTE laps than on non-VTE laps ($F(1,58) = 103.26$, p = 0.0000, ANOVA) (Figure 1D), but we did not find a significant difference in running speed (in centimeters per second) between saline and clonidine conditions ($F(1,58) = 1.64$, p = 0.21, ANOVA) (Figure 1D).

Although behavioral analyses indicated that amount of deliberation during VTE was not different between saline and clonidine, our previous study found that clonidine suppressed the alternating prospective spatial representations usually observed during VTE in hippocampus, even when rats behaviorally showed VTE (Amemiya and Redish, 2016). Therefore, we examined how oscillations were affected by clonidine during VTE to determine the underlying oscillatory components of deliberative processes. We calculated the local field potential (LFP) from the CA1 region of hippocampus in VTE and non-VTE laps during the task (17 sessions in saline and 18 sessions in clonidine). We examined four bands of oscillation components (Figures 1E–1J): theta (6–12 Hz), low gamma ([LG], 30–55 Hz), high gamma ([HG], 60–90 Hz), and epsilon (100–140 Hz) (Figures 1E and 1F). There were no differences in the average power of these oscillations between saline and clonidine across the task ($F(1,33) = 1.17$, p = 0.29 for theta; $F(1,33) = 1.56$, p = 0.22 for LG; $F(1,33) = 2.01$, p = 0.17 for HG; $F(1,33) = 2.02$, p = 0.17 for epsilon; ANOVA) (Figures 1G–1J). We applied pre-planned comparisons of power of these oscillations between non-VTE laps and VTE laps over positions to investigate how clonidine affected neural processes while rats expressed VTE. On VTE laps relative to non-VTE laps, in saline, LG and HG power increased, but neither theta nor epsilon changed (p < 0.05, false discovery rate [FDR]-corrected paired t test) (Figures 1G–1J, left). Clonidine suppressed the increase in LG and HG power seen under saline control on VTE laps (Figures 1H and 1I), suggesting both LG and HG relate to deliberative processes.

Previous studies have reported that LG and HG in CA1 are modulated by the phase of theta oscillation (Belluscio et al., 2012; Colgin et al., 2009). Therefore, we examined the relationship between theta phase and gamma power. We calculated theta phase based on the actual waveform, because the theta oscillation is asymmetric, not sinusoidal (Belluscio et al., 2012; Buzsáki et al., 1985). We calculated theta phase from the hippocampal fissure, where the amplitude of theta was the highest (Figure S1A). We defined peaks of theta as 0° and troughs of theta as 180°. Phase-amplitude analyses found that waveform phase aligned the peak of LG and HG (Figures S1C and S1D), which was quantitatively validated by the modulation index (MI) ($F(1,33) = 9.56$, p = 0.004 for LG; $F(1,33) = 83.50$, p = 0.0001 for HG; ANOVA) (Figures S1E and S1F) (Tort et al., 2009).

Consistent with previous studies (Belluscio et al., 2012; Colgin et al., 2009), phase-amplitude analyses revealed that the peaks of LG and HG power appeared at different phases of theta (Figure 2A; Figure S1A), with LG and HG preferring the ascending part and descending part of theta, respectively (Figure 2B). In saline during VTE, LG and HG power increased over theta phase (36 bins by each 10°) compared to non-VTE laps ($F(1,16) = 27.60$, $p = 0.0001$ for LG [40–55 Hz]; $F(1,16) = 12.21$, $p = 0.000$ for HG [60–90 Hz]; ANOVA) (Figures 2D and 2F). In clonidine during VTE, LG power increased over the phase relative to non-VTE laps ($F(1,17) = 24.69$, $p = 0.0001$, ANOVA) (Figure 2E), but HG power did not ($F(1,17) = 3.25$, $p = 0.089$, ANOVA) (Figure 2G). Furthermore, we examined the increases in power of gamma oscillations on VTE laps against non-VTE laps. On VTE laps, the increase in LG power in the ascending part of theta was higher in saline than in clonidine (drug condition: $F(1,33) = 2.67$, $p = 0.11$; drug × phase of theta interaction: $F(35,1,155) = 1.60$, $p = 0.015$; ANOVA) ($p < 0.05$, post hoc test with simple main effect) (Figure 2H). In contrast, the increase in HG power on VTE laps was higher in saline than in clonidine across the phase of theta (drug condition: $F(1,33) = 4.32$, $p = 0.046$; drug × phase of theta interaction: $F(35,1,155) = 0.97$, $p = 0.053$; ANOVA) and remained prominent in the descending phase of theta (Figure 2I).

We next applied phase-amplitude analyses to other areas on the maze: the navigation sequence (NS), the forward path (FP) after the choice point (CP) to the side feeder, and the side path (SP) after the side to the center feeder, in addition to at the choice point (Figure S2A), and found position-dependency coupling between theta and other oscillations. The preferred theta phase of LG and HG was relatively constant across these maze components (Figures S2B–S2E), and increases in power of LG and HG were prominent at the choice point (Figures S2B–S2E). The increase in LG power on VTE laps in saline was preserved across the FP (Figure S2F). Although there were phase-amplitude changes across the task, there were no phase-amplitude or asymmetry differences across the three contingencies of the task (left for reward, right for reward, or alternating for reward) (see Experimental Procedures).

Calculating theta phase based on actual asymmetric theta waves allowed us to evaluate the skewness of each theta wave. We calculated the asymmetry index (AI) as log[length of ascending part of theta wave] – log[length of descending part of theta wave] and analyzed it over sessions (30 sessions in saline and 30 sessions in clonidine). Most theta cycles had a longer descending part than ascending part (median AI = −0.56 in saline and −0.58 in clonidine at the choice point, −0.56 in saline and −0.56 in clonidine throughout the maze, both significantly <−0.5 [CP: $z = 43.99$, $p = 0.00$, in saline, and $z = 39.10$, $p = 0.00$, in clonidine; throughout maze: $z = 48.42$, $p = 0.00$, in saline, and $z = 42.29$, $p = 0.00$, in clonidine; signed rank test]) (Figures 3A and 3B). In saline, AI decreased as rats accessed the choice point, reaching the lowest point just before the choice point, and then increased on non-VTE laps. The decrease in AI near the choice point clearly shifted higher on VTE laps than on non-VTE laps (more symmetric) (VTE × position interaction: $F(64,1,856) = 3.29$, $p < 0.0001$, ANOVA) (Figure 3C). In clonidine, the asymmetry index decreased toward the choice point and reached at the lowest point near the choice point on non-VTE laps, and although the shift of AI higher during VTE was statistically significant (VTE × position interaction: $F(64,1,856) = 1.79$, $p = 0.0002$, ANOVA) (Figure 3D), the shift of AI during

VTE was smaller in clonidine than in saline around the choice point (drug × position interaction: $F(64,3,712) = 1.36$, $p = 0.032$, $p < 0.05$, simple main effect) (Figure 3E).

The theta period was longer on VTE laps than non-VTE laps in saline (VTE × position [64 spatial bins] interaction: $F(63,1,827) = 1.80$, $p=0.0002$, ANOVA) (Figure S3A). Previous work has shown that this is not an effect of running speed (Papale et al., 2016). Clonidine suppressed the shift of theta frequency during VTE (VTE × position interaction: $F(63,1,827) = 1.00$, $p = 0.48$) (Figure S3B). Furthermore, in saline, corresponding to the change of AI, the descending part of theta was shorter and the ascending part longer on VTE laps than non-VTE laps (VTE × position interaction: $F(63,1,827) = 2.03$, $p < 0.0001$ for descending part; $F(63,1,827) = 3.03$, $p < 0.0001$ for ascending part; ANOVA) (Figure S3C), and the change of ascending part (LG-preferred part) was more prominent than of the descending part (HG-preferred part). Clonidine suppressed these changes (VTE × position interaction: $F(63,1,827) = 1.18$, $p = 0.16$ for descending part; $F(63,1,827) = 1.55$, $p = 0.004$ for ascending part; ANOVA, but no significant difference with post hoc FDR-corrected t test) (Figure S3D).

These data suggest that the shape of theta reflects information processing. It has been reported that LG and HG power in the hippocampal CA1 region reflect different spatial information sent to CA1 from different input sources (Bieri et al., 2014; Colgin et al., 2009; Zheng et al., 2016). To examine the relationships among LG power, HG power, theta asymmetry, and information processing, we calculated the relationship between the AI and the gamma power ratio (LG/HG) for theta cycles with at least one gamma event (>2 SD). The LG/HG gamma power ratio was higher in more symmetric theta (AI > −0.5) than in more asymmetric theta (AI < −0.5) in saline ($t(16) = 6.33$, $p < 0.00001$, t test, two sided) (Figure 3F). This relationship between the AI and the gamma ratio was preserved under clonidine ($t(17) = 6.33$, $p < 0.0001$, t test, two sided, Figure 3G). Altogether, asymmetric theta, which has a relatively longer descending part (HG-preferred part), reflects HG dominance, and symmetric theta, which has a relatively longer ascending part (LG-preferred part), reflects LG dominance.

Neural activity in each theta cycle represents a short path that begins just behind the animal and ends in front of the animal as a sequence of place cell firing (Foster and Wilson, 2007; Gupta et al., 2012; Wikenheiser and Redish, 2015). At the individual cell level, the sequence is evident as phase modulation in firing by position (a place cell that has a place field in more a forward place activates during the later phase of a theta wave), which produces a phenomenon called phase precession (O'Keefe and Recce, 1993). However, as noted earlier, the theta cycles are not sine waves but rather are asymmetric (Belluscio et al., 2012). We examined the relationship between activity of place cells and theta asymmetry and determined that this asymmetry reflects changes in information processing. We examined phase precession between asymmetric and symmetric theta (Figures 4A and 4B). The descending phase corresponded to earlier positions in place fields, and the ascending phase corresponded to later (forward) positions in place fields (Figure 4A). Thus, phase precession was preserved under clonidine (Figure 4B).

In asymmetric theta waves, a large number of spikes occurred in the descending part, or HG-preferred phase, of theta. In symmetric theta waves, spikes occurred more uniformly over the phases, that is, relatively increased in the ascending part, or LG-preferred phase, of theta (Figures 4A and 4B; Figure S4). However, the difference of distribution of spikes could be attributed to the theta asymmetry (e.g., the higher number of spikes in the descending part than in the ascending part could have simply been due to an asymmetric theta cycle having a longer descending part than ascending part). Therefore, we normalized the number of spikes in a place field by total occupancy (time spent in each position in a place field) as a firing rate of place cell in its place field (saline asymmetric, n = 197; saline symmetric, n = 184; clonidine asymmetric, n = 208; clonidine symmetric, n = 226). Even after this normalization, firing rates in asymmetric theta was higher than in symmetric theta ($F(1,811) = 13.32$, $p = 0.003$, ANOVA) (Figure 4C). In asymmetric theta, there was no significant difference of firing rate between saline and clonidine across positions in place fields ($F(1,403) = 0.44$, $p = 0.50$, ANOVA) (Figure 4C, left). However, in symmetric theta, clonidine suppressed the firing rate of place cells in the ascending half of place fields ($F(24,9,792) = 2.73$, $p = 0.0001$, ANOVA) (Figure 4C, right). Altogether, these data imply that clonidine affected the firing sequence of place cells, but not phase precession, suggesting clonidine affects the content of spatial representation without disrupting basic mechanisms of place cell organization.

To determine the effect of clonidine on spatial representations, we evaluated spatial representations in each theta cycle by applying a one-step Bayesian spatial decoding algorithm to the recorded neural ensemble activity and averaged in each session (Wilson and McNaughton, 1993; Zhang et al., 1998). We decoded rats' position in both drug conditions and compared it to the rats' current position (effect of position [25 spatial bins, −42 cm to +42 cm distance from rats' position]: $F(24,288) = 84.97$, $p = 0.0000$ for saline, 13 sessions; $F(24,312) = 118.66$, $p = 0.0000$ for clonidine, 14 sessions) (Figures 5A and 5B). We found a position-dependent difference of the distribution of decoding probability between asymmetric theta and symmetric theta in saline (theta type [asymmetric or symmetric] × position interaction: $F(24,312) = 4.80$, $p = 0.000$) (Figure 5A), but not in clonidine (theta type [asymmetric or symmetric] × position interaction: $F(24,312) = 1.40$, $p = 0.11$) (Figure 5B). To clearly visualize the difference of distribution of decoding probability between asymmetric theta and symmetric theta, we calculated the difference of spatial representation between asymmetric theta and symmetric theta (Figure 5C). In saline, theta asymmetry clearly dissociated spatial representations; asymmetric theta preferentially represented rats' current position (negative value), but symmetric theta preferentially represented future position (positive value) (Figure 5C, blue line). Clonidine disrupted the differences in spatial representation between asymmetric and symmetric theta and made the distance of forward representation shorter (Figure 5C, red line).

DISCUSSION

Hippocampal spatial representations within each theta cycle progress from the current position to potential future locations. We found that theta oscillations modulated gamma power not only through the timing of their occurrence but also through changes in the relative power between low gamma (LG) and high gamma (HG). These were directly observable through the intrinsic asymmetry of theta waves: asymmetric theta cycles were

HG dominant, and symmetric theta cycles were LG dominant. The dominance of LG or HG reflected spatial representations of ensemble activity of hippocampal cells: asymmetric theta waves (HG dominant) processed current location, and symmetric theta waves (LG dominant) processed future locations. Furthermore, deliberative processes at the choice point were accompanied by increases in both LG and HG power in their corresponding theta phases and a shift to more symmetric LG-dominant theta cycles. Clonidine, which is known to suppress planning and prospective processes in a decision making, disrupted these theta-gamma relationships, revealing a disruption in the underlying hippocampal neural mechanisms that dynamically construct spatial representations from present to future within each theta cycle.

We found that pause and re-orient behaviors (vicarious trial and error [VTE]) were associated with an increase in power of both HG and LG. HG and LG in the hippocampal CA1 reflect different information transfer from the entorhinal cortex and CA3 region of the hippocampus, respectively (Colgin et al., 2009; Fries, 2005). HG in CA1 is involved in representation and recognition of current location (Brun et al., 2002), and LG in CA1 is involved in memory processing (Brun et al., 2002; Shirvalkar et al., 2010; Tort et al., 2009). The coupling revealed by gamma between CA3 and CA1 and between entorhinal cortex and CA1 was modulated depending on task demand and state (Kemere et al., 2013; Montgomery and Buzsáki, 2007), suggesting information transmissions in the CA3-CA1 circuit and in the entorhinal-CA1 circuit are modulated depending on demand. Whereas hippocampal neural activity usually represents location around an animal's position along the path, when rats show VTE, hippocampal spatial representation shifts forward from the current position, which seems to reflect mental navigation and planning processes (Redish, 2016). To navigate and plan, animals use information about previous experiences (Buzsáki and Moser, 2013; Eichenbaum, 2017), which is likely transmitted from CA3 via LG. To use the experience information, animals need to localize and recognize the current situation based on sensory cues and landmarks (Buzsáki and Moser, 2013; McNaughton et al., 2006; Muzzio et al., 2009), which may be transmitted from entorhinal as HG. The increase in power of LG and HG during VTE would thus reflect information processes to create non-local spatial representations in reference to the current location.

Our data support a relationship between phase precession and theta modulation of gamma oscillations (Bieri et al., 2014; Cabral et al., 2014; Lasztóczi and Klausberger, 2016). These hypotheses imply that place cell spikes reflect different information processes depending on the theta phase of the spikes. Consistent with previous studies (Bieri et al., 2014; Cabral et al., 2014; Fernández-Ruiz et al., 2017; Lasztóczi and Klausberger, 2016), we observed that what separates sensory and memory processing is the gamma component occurring at different phases of theta.

Our results suggest that the intrinsic asymmetry of theta cycles reflects information processing in theta cycles. The asymmetry of theta waves reflects the dominance of power between high gamma and low gamma components. Previous studies have reported that the LG state associates with prospective coding and the HG state associates with coding of the current location (Bieri et al., 2014; Cabral et al., 2014). Our data reveal that intrinsic asymmetry of theta cycles reflects the gamma states: more asymmetric theta with a relatively longer HG phase reflects preference for current location representations, and more

symmetric theta with a relatively longer LG phase reflects farther search processes. Associated with these different theta wave shapes, ensemble activity of cells in asymmetric theta cycles preferentially represents the current location, and ensemble activity of cells in symmetric theta cycles preferentially represents future locations.

Similarly, it has been found that sequences go farther during vicarious trial and error (VTE) events than during smooth running behavior (Johnson and Redish, 2007; Papale et al., 2016). We found that VTE behaviors were associated with more symmetric theta, suggesting a mechanism by which VTE entailed future search processes. In our data, more symmetric theta waves represented more forward locations. This is supported by the observation that theta periods become longer with the shift to more symmetric theta (Figure S3).

Furthermore, we found that the asymmetry of theta cycles changed depending on where in the maze the animal was, which may reflect differences in what spaces were represented during those theta sequences. As animals approach landmarks such as choice points and feeders, theta sequences tend to include the immediate past location, and as animals leave the landmark, theta sequences tend to include future locations (Gupta et al., 2012). In our data, theta cycle shape became more asymmetric as animals approached the landmarks, notably the choice point, and shifted to be more symmetric just after leaving the choice point (Figure 3C), implying a change in representation as the animal passed the landmark.

Our data also suggest that noradrenergic manipulations drive a shift of the gamma state toward a more prospective mode. Noradrenaline enhances LG power in CA1 (Hajós et al., 2003) and plays a role in excitation of CA3 neural networks (Haggerty et al., 2013; Jurgens et al., 2005). It also plays a role in memory retrieval (Devauges and Sara, 1991; Murchison et al., 2004; Sara and Devauges, 1989). These studies suggest that noradrenaline induces an LG-preferring state (more symmetric theta) by increasing LG input from CA3 to CA1 (Pietersen et al., 2014). This is supported by our findings that clonidine suppressed place cells' firing relating, on entrance, to the place field during LG-preferred theta phases, and shifted the theta waves to be more symmetric, associated with more prominent prolongation of the LG-preferred part of theta waves rather than shortening of the HG-preferred part (Figure S3C). However, clonidine suppressed HG during VTE, as well as LG, and a few studies have reported a relationship between noradrenaline and HG in the hippocampal CA1 (Wójtowicz et al., 2009), suggesting that noradrenergic modulation of the gamma state may be more complex than a simple change in CA3-CA1 coupling.

It has been hypothesized that theta waves organize the hippocampal spatial representation from multiple information conveyed by gamma oscillations. Studies have reported that the transition from present to future in the hippocampal spatial representation varies with state and demand. Our data suggest that theta modulation of the transition between gamma oscillations dynamically constructs the spatial representations, which is predicted by dynamic changes in the intrinsic shape of each theta cycle. Furthermore, noradrenaline can be a modulator of the dynamic information processes in theta-gamma coupling and can induce deliberative, planning, and imaginative processes.

EXPERIMENTAL PROCEDURES

Subjects

Male Fisher-Brown Norway hybrid (FBNF-1) rats, age 11–17 months at the time of implantation (n = 4), were maintained on a 12:12 hr light-dark cycle. Rats were food restricted to no less than 80% of their body weight during behavioral training, and water was freely available in the home cage at all times. All procedures were conducted in accordance with NIH guidelines for animal care and approved by the Institutional Animal Care and Use Committee (IACUC) at the University of Minnesota. Care was taken to minimize the number of animals used in these experiments and to minimize suffering.

Task

Rats were trained to perform a modified version of a Hebb-Williams maze (HWM) (Hebb and Williams, 1946). The maze was a wooden rectangular box with carpeted floor and Duplo brick walls that could be altered to change the internal maze portion (Figure 1A). At the end of a changeable central path, rats came to a choice point (CP) and had to make a left or right turn. If they made the correct choice, they received a food reward (two unflavored food pellets, 45 mg each; Research Diets, New Brunswick, NJ, USA) at the corresponding side feeder (Fs) location and at the center feeder (Fc) location. The pellets were delivered using automatic pellet dispensers (Med-Associates, St. Albans, VT, USA). If the rat made the wrong choice, no pellet was delivered at either the side feeder location or the center feeder location. Three reward contingencies were used: turn left at CP (L contingency), turn right at CP (R contingency), or alternate between sides (A contingency). The alternation contingency required the rat to run to the side opposite the most recently rewarded side. During training sessions, the reward contingency was held constant through an entire session but changed randomly from session to session. Rats ran the task continuously for 30 min on each daily training session. Probe sessions lasted 40 min. During the probe test sessions, each session began with one reward contingency, but the reward contingency changed after approximately 20 min, which was approximately the halfway point of the session. No external cues were provided to signal the change in reward contingency (beyond lack of delivery of the expected reward). Rats ran a subset of the six possible combinations of left (L), right (R), and alternation (A) contingencies (LR, LA, RL, RA, AL, and AR), pseudorandomly. The central path remained constant throughout a given session, including both reward contingencies of a probe session, but changed from session to session.

Surgery and Tetrode Placement

After pre-training on the HWM, rats were chronically implanted with 14-tetrode hyperdrives (12 electrodes for recording and 2 electrodes for references) targeting the right CA1 region of dorsal hippocampus (3.8 mm posterior and 3.0 mm right-lateral from bregma). The details of the surgery have been described previously (Regier et al., 2015). Following the surgery, tetrodes and references were slowly advanced toward the pyramidal cell layer over approximately 2 weeks. The hippocampal pyramidal layer was identified by the size and reversal of sharp-wave ripples, as well as by burst firing of cells in synchrony with the ripple portions of the sharp-wave ripple complexes. One reference was lowered to the hippocampal

fissure for theta detection, and the other was left in corpus callosum or a quiet region of cortex to be used as a superficial reference.

Data Collection

Neural data were recorded by a 64-channel Neuralynx Cheetah system (Bozeman, MT), and an overhead camera tracked subject position via light emitting diodes (LEDs) on the headstage. LFPs were sampled at 2 kHz and bandpass filtered from 1 to 475 Hz. Spike trains were identified and recorded online using built-in filters, filtered from 600 to 6,000 Hz, and then spikes were clustered offline. Neurons were separated into putative cells on the basis of specific waveform properties using KlustaKwik (K.D. Harris) and MClust 3.5 or MClust 4.0 (A.D.R.). Only clusters well separated from others and/or with $L_{ratio} < 0.15$ were used for analysis. Recording sessions consisted of 2–3 non-switch sessions per rat and 12–15 switch sessions per rat under pharmacological manipulation (clonidine) or vehicle control (saline).

Pharmacological Manipulation

Clonidine hydrochloride (Sigma-Aldrich, St. Louis, MO, USA), an alpha-2 autoreceptor agonist, was dissolved in saline and injected at a dosage of 30 μg/kg. Saline vehicle was used as a control. For the recording sessions, clonidine or saline vehicle was intraperitoneally injected 30 min before the rat was placed on the track. The rat rested in its home cage for those 30 min. The order of injection of either clonidine or saline was randomly assigned in each rat, and the investigator was blind to which was injected.

Histology

After the experiment was completed, tetrode locations were marked with small lesions by passing a small amount of anodal current (5 μA for 10 s) through each tetrode. After at least 2 days had passed, rats were anesthetized and perfused transcardially with saline followed by 10% formalin. Brains were stored in formalin followed by 30% sucrose formalin until slicing. Coronal slices were made through the area of the implantation and stained with cresyl violet to visualize tetrode tracks.

Data Analysis

zIdPhi Measurement—Vicarious trial and error (VTE) was quantified by calculating *zIdPhi*, the *Z*-scored integrated angular velocity across a pass through the choice point (Papale et al., 2012). Briefly, a pass through the choice point was defined by the sequence of <x,y> coordinates as the rat ran through the choice area of the maze covering the choice point. The orientation of motion was found by applying the Janabi-Sharifi algorithm (Janabi-Sharifi et al., 2000) to the <x,y> sequence to determine <dx,dy> and taking the arctangent of <dx,dy> to determine the orientation of motion <phi>. The change in orientation of motion <dphi> was calculated by applying the Janabi-Sharifi algorithm to the <phi> sequence. The absolute value of <dphi> was calculated and integrated across the entire pass to produce an *IdPhi* for a given pass. Left and right passes were separately *Z* scored within each session to produce a zIdPhi measure for each pass through the choice point, because the path through the choice point can have a different baseline of integrated absolute angular velocity

depending on the specific path required by the changeable central path (maze portion) used in a given day. zIdPhi values greater than 0.5 were defined as VTE events.

Linearization of Maze—The maze was linearized using manual marking of the key landmarks and linear interpolation between those marks (Schmitzer-Torbert and Redish, 2004). The maze was linearized into 65 samples to the left and right side paths separately (Gupta et al., 2012). Thus, the maze was divided into 65×2 spatial bins.

Power Spectral Analyses across Position—For spectral analysis of oscillations across positions on the maze, we calculated power spectral density (PSD) by multi-taper Fourier analysis using the MATLAB tool box Chronux function mtspectrumc.m, setting a window length of 1 s with a taper of [3 5] and with frequencies ranging from 1 to 300 Hz and assigned into positions (65 bins) on the linearized maze. To quantify oscillation bands, the PSD averaged in a range of theta (6–12 Hz), LG (30–55 Hz), HG (60–90 Hz), and epsilon (100–140 Hz) bands on non-VTE and VTE laps.

Theta Wave Analyses—To identify theta characteristics, theta cycles were determined based on waveform-based theta as previously reported (Belluscio et al., 2012). To detect theta cycles, a bandpass filter (1–80 Hz) was applied to the LFP trace recorded from the hippocampal fissure, and local minima and maxima in the theta range (6–12 Hz) were determined as peaks and trough of theta, respectively. Theta cycles were defined as the time between the peaks, and theta phases were defined for peaks of the signal as 0 and for troughs as 180. Theta frequency and the length of the ascending part and the descending part of theta cycles were calculated based on the waveform theta.

In comparison to waveform-based theta, theta as a sigmoidal sine wave, which has often been studied, was determined by Hilbert transformation of the bandpass-filtered theta band (6–12 Hz). The relationship of phase between waveform theta and bandpass theta was quantified as a histogram of waveform phase $\times$ bandpass phase.

Detection of Gamma Events—To detect theta cycles associated with gamma activity, power within the frequency bands for LG (30–55 Hz) and HG (60–90 Hz) was calculated by Hilbert transformation. Time points of peaks of the LG and HG that exceeded 2 SDs above the averaged power of LG and HG were collected.

Theta Phase and Power Spectral Coupling Analysis—To examine the relationship between theta phase and power of spectra, the averaged power of spectra over theta phase was calculated. Time-varying power of spectra was computed by applying a Morlet wavelet analysis over a frequency range (20–300 Hz) and was normalized in each frequency. The power of spectra in time points that corresponded to each theta phase was averaged over frequencies. To quantify theta phase-gamma power coupling, we calculated the modulation index (MI) in theta cycles with gamma events (Tort et al., 2010).

Gamma Power Ratio Analysis—Power ratios of low gamma (LG) and high gamma (HG) were calculated for theta cycles with a running speed > 5 cm/s. The spectral power for LG and HG was calculated by Hilbert transformation. The individual power was averaged in

each frequency window. The gamma power ratio in theta cycles was calculated as the averaged power of LG divided by the averaged power of HG in each theta cycle.

Place Field Detection—Place fields were calculated from spikes recorded when the animal's running speed was >5 cm/s. Units with a mean firing rate < 0.04 Hz (non-task-responsive cells) or a mean firing rate > 4 Hz (putative interneurons) after the exclusion of spikes were excluded from further analyses. The spatial tuning curves of cells were calculated into the linearized maze (65×2 bins). Place fields were then identified as contiguous bins in which the firing rate was   10% of the cell's session maximum firing rate. Fields separated by <3.5 cm were merged.

Relationship of Place Cell Firing to Theta Phase and Position in Place Fields—For each time point of spikes of place cells in each place field, the correspondent theta phase and the normalized position in the place field were calculated. Sizes of place fields were normalized and divided into 25 bins. Phase precession was calculated as a histogram of the firing phase versus the normalized position using all collected spikes from all place fields.

Phase versus spike analyses were examined by counting the number of spikes over theta phases. The firing rate was calculated as [number of spikes/spending time] in each position in place fields and then smoothed with a sliding window of 11 spatial bins.

Spatial Decoding in Theta Cycles—To examine the spatial representation in theta cycles, we used a Bayesian spatial decoding algorithm (Zhang et al., 1998) applied to the linearized maze. We decoded spiking in each theta cycle to obtain a probability distribution across the linearized maze. The obtained probability distributions of theta cycles were aligned at a rat's current position as 0 cm. Sessions with at least 11 simultaneously recorded cells were used for this analysis (13 sessions in saline and 14 sessions in clonidine). Theta cycles including at least one spike and a running speed faster than 5 cm/s were used for this analysis.

Statistics—For any two group comparisons, a rank-sum test was used. To assess position-dependent changes in the behavioral and LFP data, two-way ANOVA [lap type (VTE/non-VTE) as factor × position as repeated measure] was used, followed by a post hoc FDR-corrected t test. For LFP across theta phase analysis and place cell firing across place field, two-way ANOVA [lap type (VTE/non-VTE) as factor × theta phase or position as repeated measure] was used, followed by a simple main effects test for further post hoc analyses. For decoding data, two-way ANOVA [theta asymmetry as factor × position as repeated measure] was used. A signed rank test was used to examine the difference in decoding probability between asymmetry theta and symmetry theta.

Supplementary Material

Refer to Web version on PubMed Central for supplementary material.

Acknowledgments

References

Amemiya S, Redish AD. Manipulating decisiveness in decision making: effects of clonidine on hippocampal search strategies. J. Neurosci. 2016; 36:814–827. [PubMed: 26791212]

Amemiya S, Noji T, Kubota N, Nishijima T, Kita I. Noradrenergic modulation of vicarious trial-and-error behavior during a spatial decision-making task in rats. Neuroscience. 2014; 265:291–301. [PubMed: 24480363]

Belluscio MA, Mizuseki K, Schmidt R, Kempter R, Buzsáki G. Cross-frequency phase-phase coupling between θ and γ oscillations in the hippocampus. J. Neurosci. 2012; 32:423–435. [PubMed: 22238079]

Bieri KW, Bobbitt KN, Colgin LL. Slow and fast γ rhythms co-ordinate different spatial coding modes in hippocampal place cells. Neuron. 2014; 82:670–681. [PubMed: 24746420]

Brun VH, Otnass MK, Molden S, Steffenach HA, Witter MP, Moser MB, Moser EI. Place cells and place recognition maintained by direct entorhinal-hippocampal circuitry. Science. 2002; 296:2243–2246. [PubMed: 12077421]

Buzsáki G, Moser EI. Memory, navigation and theta rhythm in the hippocampal-entorhinal system. Nat. Neurosci. 2013; 16:130–138. [PubMed: 23354386]

Buzsáki G, Rappelsberger P, Kellényi L. Depth profiles of hippocampal rhythmic slow activity ('theta rhythm') depend on behaviour. Electroencephalogr. Clin. Neurophysiol. 1985; 61:77–88.

Cabral HO, Vinck M, Fouquet C, Pennartz CM, Rondi-Reig L, Battaglia FP. Oscillatory dynamics and place field maps reflect hippocampal ensemble processing of sequence and place memory under NMDA receptor control. Neuron. 2014; 81:402–415. [PubMed: 24462101]

Cohen, NJ., Eichenbaum, H. Memory, Amnesia, and the Hippocampal System. MIT Press; 1993.

Colgin LL, Denninger T, Fyhn M, Hafting T, Bonnevie T, Jensen O, Moser M-B, Moser EI. Frequency of gamma oscillations routes flow of information in the hippocampus. Nature. 2009; 462:353–357. [PubMed: 19924214]

Devauges V, Sara SJ. Memory retrieval enhancement by locus coeruleus stimulation: evidence for mediation by beta-receptors. Behav. Brain Res. 1991; 43:93–97. [PubMed: 1650233]

Eichenbaum H. The role of the hippocampus in navigation is memory. J. Neurophysiol. 2017; 117:1785–1796. [PubMed: 28148640]

Fernández-Ruiz A, Oliva A, Nagy GA, Maurer AP, Berényi A, Buzsáki G. Entorhinal-CA3 dual-input control of spike timing in the hippocampus by theta-gamma coupling. Neuron. 2017; 93:1213–1226. [PubMed: 28279355]

Foster DJ, Wilson MA. Hippocampal theta sequences. Hippocampus. 2007; 17:1093–1099. [PubMed: 17663452]

Fries P. A mechanism for cognitive dynamics: neuronal communication through neuronal coherence. Trends Cogn. Sci. 2005; 9:474–480. [PubMed: 16150631]

Gupta AS, van der Meer MA, Touretzky DS, Redish AD. Segmentation of spatial experience by hippocampal θ sequences. Nat. Neuro-sci. 2012; 15:1032–1039.

Haggerty DC, Glykos V, Adams NE, Lebeau FE. Bidirectional modulation of hippocampal gamma (20–80 Hz) frequency activity *in vitro* via alpha(α)- and beta(β)-adrenergic receptors (AR). Neuroscience. 2013; 253:142–154. [PubMed: 23994151]

Hajós M, Hoffmann WE, Robinson DD, Yu JH, Hajós-Korcsok E. Norepinephrine but not serotonin reuptake inhibitors enhance theta and gamma activity of the septo-hippocampal system. Neuropsychopharmacology. 2003; 28:857–864. [PubMed: 12637957]

Hassabis D, Maguire EA. Deconstructing episodic memory with construction. Trends Cogn. Sci. 2007; 11:299–306. [PubMed: 17548229]

Hebb DO, Williams K. A method of rating animal intelligence. J. Gen. Psychol. 1946; 34:59–65. [PubMed: 21015350]

Janabi-Sharifi F, Hayward V, Chen JC. Discrete-time adaptive windowing for velocity estimation. IEEE Trans. Contr. Syst. Technol. 2000; 8:1003–1009.

Johnson A, Redish AD. Neural ensembles in CA3 transiently encode paths forward of the animal at a decision point. J. Neurosci. 2007; 27:12176–12189. [PubMed: 17989284]

Jurgens CW, Rau KE, Knudson CA, King JD, Carr PA, Porter JE, Doze VA. Beta1 adrenergic receptor-mediated enhancement of hippocampal CA3 network activity. J. Pharmacol. Exp. Ther. 2005; 314:552–560. [PubMed: 15908512]

Kemere C, Carr MF, Karlsson MP, Frank LM. Rapid and continuous modulation of hippocampal network state during exploration of new places. PLoS ONE. 2013; 8:e73114. [PubMed: 24023818]

Lasztóczi B, Klausberger T. Hippocampal place cells couple to three different gamma oscillations during place field traversal. Neuron. 2016; 91:34–40. [PubMed: 27387648]

Lisman J, Redish AD. Prediction, sequences and the hippocampus. Philos. Trans. R. Soc. Lond. B Biol. Sci. 2009; 364:1193–1201. [PubMed: 19528000]

Maurer AP, McNaughton BL. Network and intrinsic cellular mechanisms underlying theta phase precession of hippocampal neurons. Trends Neurosci. 2007; 30:325–333. [PubMed: 17532482]

McNaughton BL, Battaglia FP, Jensen O, Moser EI, Moser MB. Path integration and the neural basis of the 'cognitive map'. Nat. Rev. Neurosci. 2006; 7:663–678. [PubMed: 16858394]

Montgomery SM, Buzsáki G. Gamma oscillations dynamically couple hippocampal CA3 and CA1 regions during memory task performance. Proc. Natl. Acad. Sci. USA. 2007; 104:14495–14500. [PubMed: 17726109]

Murchison CF, Zhang XY, Zhang WP, Ouyang M, Lee A, Thomas SA. A distinct role for norepinephrine in memory retrieval. Cell. 2004; 117:131–143. [PubMed: 15066288]

Muzzio IA, Kentros C, Kandel E. What is remembered? Role of attention on the encoding and retrieval of hippocampal representations. J. Physiol. 2009; 587:2837–2854. [PubMed: 19525568]

O'Craven KM, Kanwisher N. Mental imagery of faces and places activates corresponding stiimulus-specific brain regions. J. Cogn. Neurosci. 2000; 12:1013–1023. [PubMed: 11177421]

O'Keefe J, Dostrovsky J. The hippocampus as a spatial map. Preliminary evidence from unit activity in the freely-moving rat. Brain Res. 1971; 34:171–175. [PubMed: 5124915]

O'Keefe, J., Nadel, L. The Hippocampus as a Cognitive Map. Oxford University Press; 1978.

O'Keefe J, Recce ML. Phase relationship between hippocampal place units and the EEG theta rhythm. Hippocampus. 1993; 3:317–330. [PubMed: 8353611]

Papale AE, Stott JJ, Powell NJ, Regier PS, Redish AD. Interactions between deliberation and delay-discounting in rats. Cogn. Affect. Behav. Neurosci. 2012; 12:513–526. [PubMed: 22588853]

Papale AE, Zielinski MC, Frank LM, Jadhav SP, Redish AD. Interplay between hippocampal sharp-wave-ripple events and vicarious trial and error behaviors in decision making. Neuron. 2016; 92:975–982. [PubMed: 27866796]

Pearson J, Naselaris T, Holmes EA, Kosslyn SM. Mental imagery: functional mechanisms and clinical applications. Trends Cogn. Sci. 2015; 19:590–602. [PubMed: 26412097]

Pietersen AN, Ward PD, Hagger-Vaughan N, Wiggins J, Jefferys JG, Vreugdenhil M. Transition between fast and slow gamma modes in rat hippocampus area CA1 *in vitro* is modulated by slow CA3 gamma oscillations. J. Physiol. 2014; 592:605–620. [PubMed: 24277864]

Redish, AD. Beyond the Cognitive Map: From Place Cells to Episodic Memory. MIT Press; 1999.

Redish AD. Vicarious trial and error. Nat. Rev. Neurosci. 2016; 17:147–159. [PubMed: 26891625]

Regier PS, Amemiya S, Redish AD. Hippocampus and subregions of the dorsal striatum respond differently to a behavioral strategy change on a spatial navigation task. J. Neurophysiol. 2015; 114:1399–1416. [PubMed: 26084902]

Sara SJ, Devauges V. Idazoxan, an alpha-2 antagonist, facilitates memory retrieval in the rat. Behav. Neural Biol. 1989; 51:401–411. [PubMed: 2543356]

Saunier CF, Akaoka H, de la Chapelle B, Charléty PJ, Chergui K, Chouvet G, Buda M, Quintin L. Activation of brain noradrenergic neurons during recovery from halothane anesthesia. Persistence of phasic activation after clonidine. Anesthesiology. 1993; 79:1072–1082. [PubMed: 8238984]

Schacter DL, Addis DR, Buckner RL. Remembering the past to imagine the future: the prospective brain. Nat. Rev. Neurosci. 2007; 8:657–661. [PubMed: 17700624]

Schmitzer-Torbert N, Redish AD. Neuronal activity in the rodent dorsal striatum in sequential navigation: separation of spatial and reward responses on the multiple T task. J. Neurophysiol. 2004; 91:2259–2272. [PubMed: 14736863]

Shirvalkar PR, Rapp PR, Shapiro ML. Bidirectional changes to hippocampal theta-gamma comodulation predict memory for recent spatial episodes. Proc. Natl. Acad. Sci. USA. 2010; 107:7054–7059. [PubMed: 20351262]

Spiers HJ, Maguire EA. Thoughts, behaviour, and brain dynamics during navigation in the real world. Neuroimage. 2006; 31:1826–1840. [PubMed: 16584892]

Sullivan D, Csicsvari J, Mizuseki K, Montgomery S, Diba K, Buzsáki G. Relationships between hippocampal sharp waves, ripples, and fast gamma oscillation: influence of dentate and entorhinal cortical activity. J. Neurosci. 2011; 31:8605–8616. [PubMed: 21653864]

Takahashi M, Nishida H, Redish AD, Lauwereyns J. Theta phase shift in spike timing and modulation of gamma oscillation: a dynamic code for spatial alternation during fixation in rat hippocampal area CA1. J. Neurophysiol. 2014; 111:1601–1614. [PubMed: 24478159]

Tort AB, Komorowski RW, Manns JR, Kopell NJ, Eichenbaum H. Theta-gamma coupling increases during the learning of item-context associations. Proc. Natl. Acad. Sci. USA. 2009; 106:20942–20947. [PubMed: 19934062]

Tort AB, Komorowski R, Eichenbaum H, Kopell N. Measuring phase-amplitude coupling between neuronal oscillations of different frequencies. J. Neurophysiol. 2010; 104:1195–1210. [PubMed: 20463205]

Vanderwolf CH. Limbic-diencephalic mechanisms of voluntary movement. Psychol. Rev. 1971; 78:83–113. [PubMed: 5547375]

Wikenheiser AM, Redish AD. Hippocampal theta sequences reflect current goals. Nat. Neurosci. 2015; 18:289–294. [PubMed: 25559082]

Wilson MA, McNaughton BL. Dynamics of the hippocampal ensemble code for space. Science. 1993; 261:1055–1058. [PubMed: 8351520]

Wójtowicz AM, van den Boom L, Chakrabarty A, Maggio N, Haq RU, Behrens CJ, Heinemann U. Monoamines block kainate- and carbachol-induced gamma-oscillations but augment stimulus-induced gamma-oscillations in rat hippocampus *in vitro*. Hippocampus. 2009; 19:273–288. [PubMed: 19173289]

Yamamoto J, Suh J, Takeuchi D, Tonegawa S. Successful execution of working memory linked to synchronized high-frequency gamma oscillations. Cell. 2014; 157:845–857. [PubMed: 24768692]

Zhang K, Ginzburg I, McNaughton BL, Sejnowski TJ. Interpreting neuronal population activity by reconstruction: unified framework with application to hippocampal place cells. J. Neurophysiol. 1998; 79:1017–1044. [PubMed: 9463459]

Zheng C, Bieri KW, Hsiao YT, Colgin LL. Spatial sequence coding differs during slow and fast gamma rhythms in the hippocampus. Neuron. 2016; 89:398–408. [PubMed: 26774162]

Highlights

- Place cells sweep from current to future locations within each theta cycle

- Sweeps depend on low gamma (30–55 Hz) and high gamma (60–90 Hz) within each theta cycle

- Clonidine (noradrenergic auto-receptor agonist) disrupts gamma power

- Clonidine correspondingly reduces representations of future locations
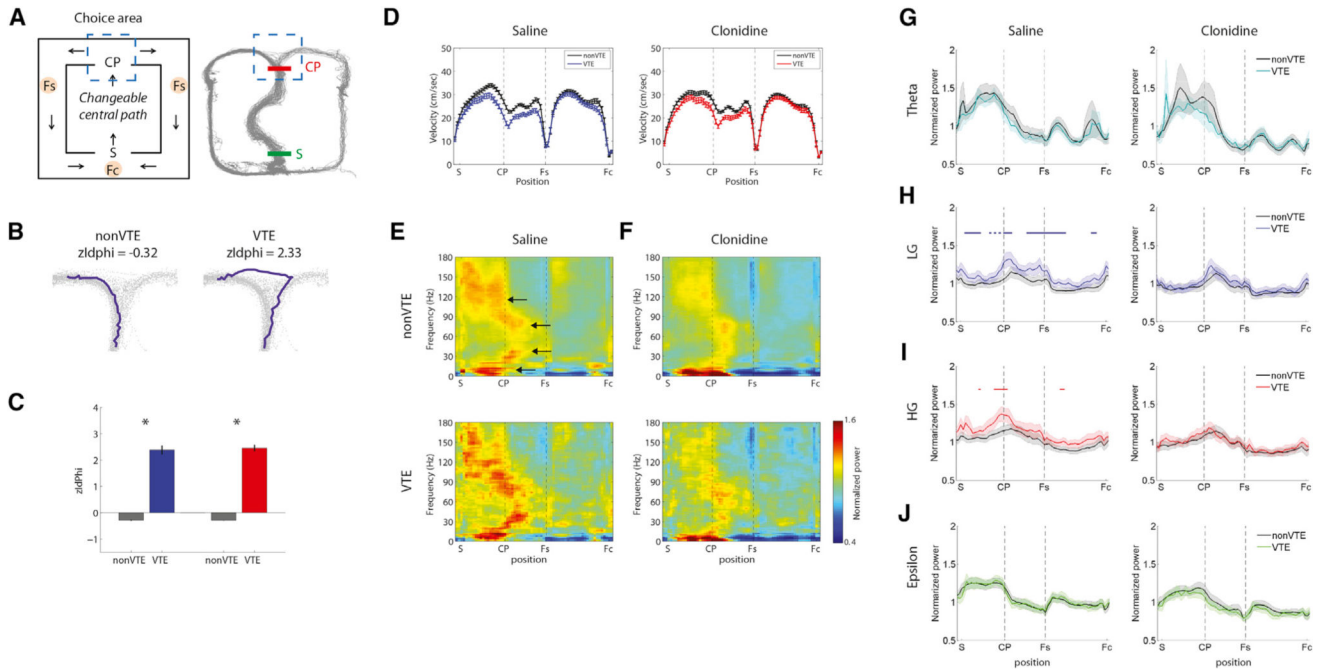
Figure 1. Clonidine Suppresses Increases in Low and High Gamma Power during VTE without Affecting Behavioral Features of VTE in a Spatial Decision-Making Task

(A) Modified Hebb-Williams maze (HWM) task. (Left) The HWM maze consisted of a changeable central path, choice point (CP), and return rails with food reward sites (Fs, side feeder; Fc, center feeder) leading back to the start (S) of the loop. (Right) An example of rat's trajectory on the HWM task. The S corresponds to the junction of left paths and right paths, and the CP was defined as a late position before the left paths and right paths separated. Blue dotted lines including CP enclose the (unmarked) choice area.

(B) Examples of trajectory of a non-VTE lap (left) and a VTE lap (right). Gray dots indicate rats' positions in the choice area for all passes in the session. Purple lines indicate the path of an animal during a single pass through the choice point. The title of each example shows the zIdPhi score for that pass.

(C) Averages of zIdPhi on non-VTE laps and VTE laps in saline (left) and clonidine (right). Mean ± SE (n = 30 sessions in saline and n = 30 sessions in clonidine). *p < 0.05, rank-sum test, two sided.

(D) Running speed on the HWM task (S, start; CP, choice point; Fs, side feeder; Fc, center feeder) on non-VTE laps and VTE laps in saline (left) and clonidine (right). Mean ± SE (n = 30 sessions in saline and n = 30 sessions in clonidine).

(E) Mean local field potential (LFP) across positions on non-VTE laps (upper) and VTE laps (lower) in saline. LFP of oscillation bands increase around the choice point on VTE laps comparing to non-VTE laps. Arrows indicate 4 oscillation bands (Bottom to top: theta, LG, HG, epsilon).

(F) Same as (E) in clonidine. Clonidine suppressed the increase in LFP of oscillation bands around the choice point during VTE.

(G–J) Comparison in LFP between non-VTE laps and VTE laps over positions in saline and clonidine. Mean ± SE (n = 17 sessions in saline and n = 18 sessions in clonidine). p < 0.05, FDR-corrected t test. (G) LFP of theta band power in saline (left) and in clonidine (right).

Black lines show theta power on non-VTE laps, and cyan lines show theta power on VTE laps. (H) Same as (G) in LG. Black lines show LG power on non-VTE laps, and blue lines show LG power on VTE laps. Blue horizontal lines show significant difference between non-VTE and VTE laps. (I) Same as (G) in HG. Blacklines show HG power on non-VTE laps, and red lines show HG power on VTE laps. Red horizontal lines show significant difference between non-VTE and VTE laps. (J) Same as (G) in epsilon band. Black lines show epsilon power on non-VTE laps, and green lines show epsilon power on VTE laps.
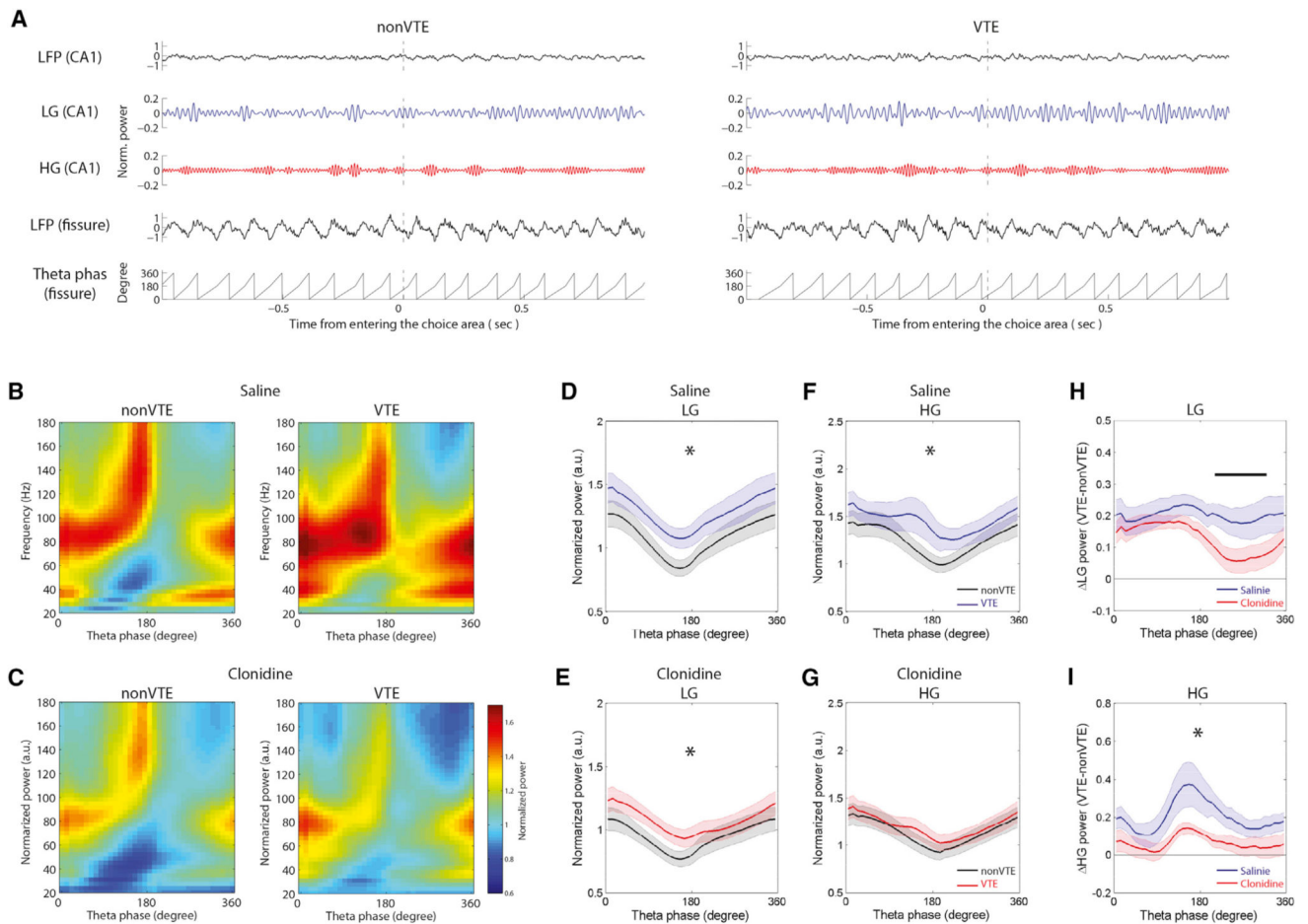
Figure 2. LG and HG Prefer Different Phase of Theta, and Clonidine Suppresses the Phase-Dependent Increase in LG and HG during VTE

(A) Examples of local field potential around the choice point on non-VTE laps (left) and VTE laps (right). Top rows represent the raw signal of the CA1 layer. Second (blue line) and third (red lines) rows represent filtered LG and HG, respectively. Fourth rows represent the raw signal of near fissure. Bottom rows represent the theta phase calculated from the hippocampal fissure. Vertical dashed lines show the time at which rats entered the choice area.

(B) Mean power of frequencies over the phase of theta in the choice area on non-VTE laps (left) and VTE laps (right) in saline. Hot color means higher power.

(C) Same as (B) in clonidine.

(D–G) Quantification of powers of LG and HG across the theta phase in the choice area. Mean ± SE (n = 17 in saline and n = 18 in clonidine). *p < 0.05, ANOVA. (D) Power of LG over theta phases in saline. Black line shows power of LG on non-VTE laps, and blue line shows power of LG on VTE laps. (E) Same as (D) in clonidine. Black line shows power of LG on non-VTE laps, and red line shows LG power on VTE laps. (F) Power of HG over theta phases in saline. Black line shows power of HG on non-VTE laps, and blue line shows power of HG on VTE laps. (G) Same as (F) in clonidine. Black line shows power of HG on non-VTE laps, and red line shows HG power on VTE laps.

(H) Differences of power of LG between non-VTE laps and VTE laps in the choice area. Blue line shows difference of power of LG between non-VTE and VTE in saline (traces shown in D). Red line shows difference of power of LG between non-VTE and VTE in clonidine (traces shown in E). Black horizontal lines show significant difference between saline and clonidine. Mean ± SE. p < 0.05, simple main effect.

(I) Differences of power of HG between non-VTE laps and VTE laps in the choice area. Blue line shows difference of power of HG between non-VTE and VTE in saline (traces shown in F). Red line shows difference of power of HG between non-VTE and VTE in clonidine (traces shown in G). Mean ± SE. *p < 0.05, ANOVA.
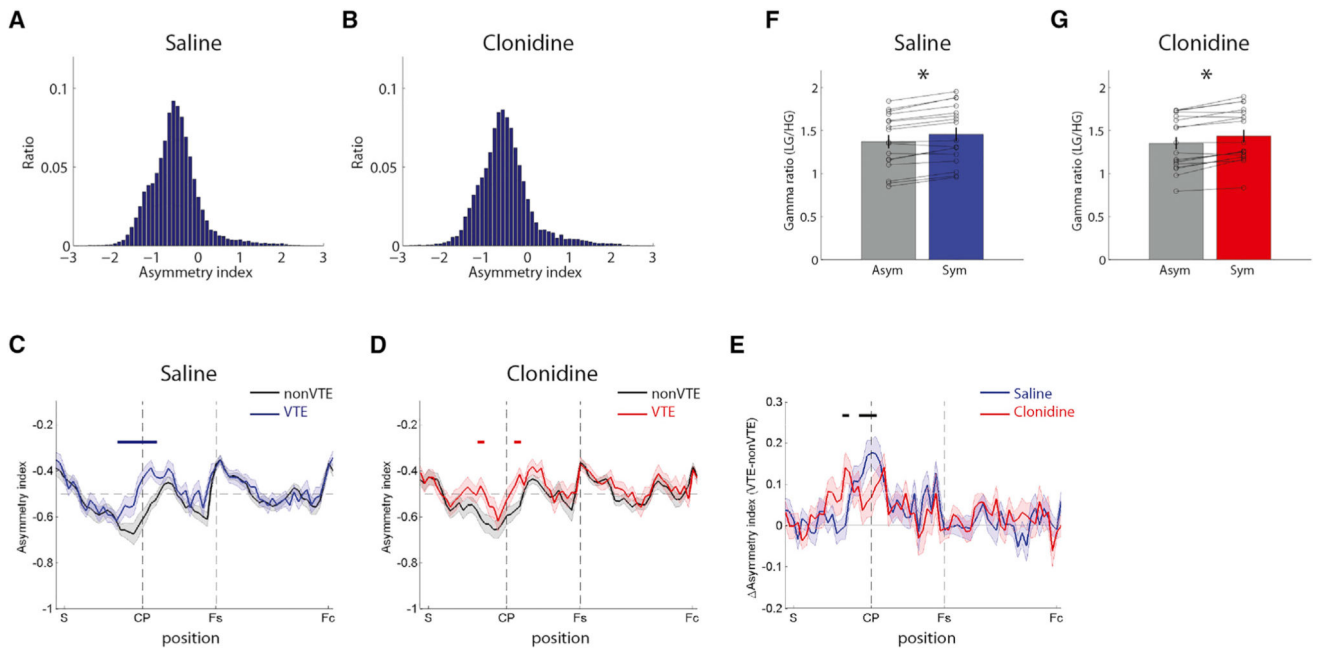
Figure 3. Shape of Theta Waves Changes Position Dependently and Reflects Gamma Components, and Clonidine Interferes with Shift of Shape of Theta during VTE

(A) Histogram of the asymmetry index (AI) of theta waves in the choice area in saline.

(B) Same as (A) in clonidine.

(C) Change of AI across positions in saline. Black line shows AI on non-VTE laps, and blue line shows AI on VTE laps (S, start; CP, choice point; Fs, side feeder; Fc, center feeder). Horizontal black dashed line shows zIdPhi = 0.5 (median). Horizontal blue solid line shows a significant difference between non-VTE laps and VTE laps. Mean ± SE (n = 30 sessions). p < 0.05, FDR-corrected t test, two sided.

(D) Same as (C) in clonidine. Black line shows AI on non-VTE laps, and red line shows AI on VTE laps. Horizontal red solid line shows a significant difference between non-VTE and VTE laps. Mean ± SE (n = 30 sessions). p < 0.05, FDR-corrected t test.

(E) Difference of asymmetry index (AI) was calculated by [AI on VTE laps – AI on non-VTE laps] in each position on the maze. Blue line shows the difference of AI in saline, and red line shows the difference of AI in clonidine. Black horizontal lines show significant difference between saline and clonidine. Mean ± SE (n = 30 sessions for saline and n = 30 sessions clonidine). p < 0.05, simple main effect.

(F) Ratio of gamma powers (LG/HG) in asymmetric (AI < −0.5) and symmetric (AI > −0.5) theta in saline. Mean ± SE (n = 17 sessions). *p < 0.05, paired t test, two sided.

(G) Same as (E) in clonidine (n = 18 sessions).
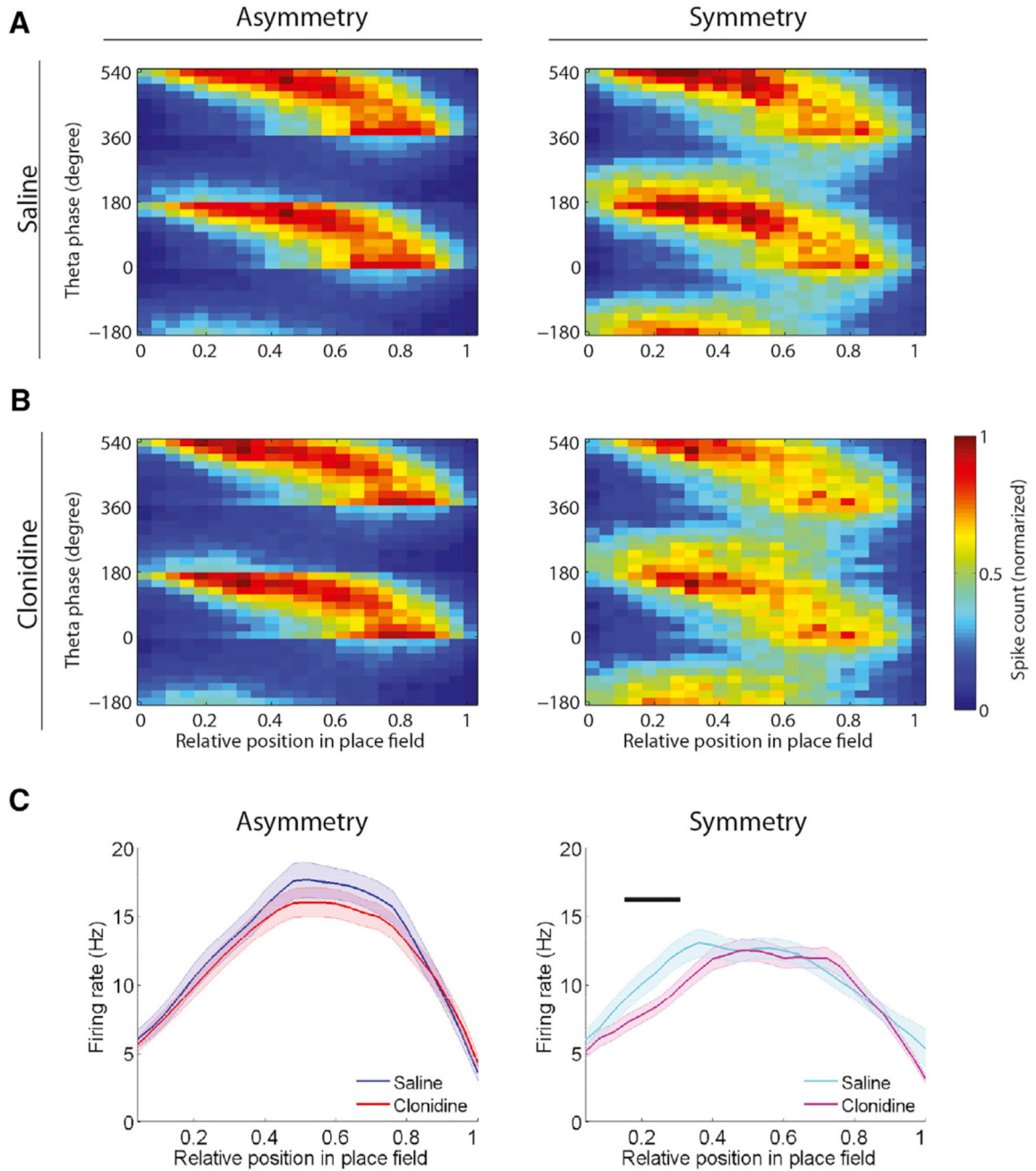
Figure 4. Shape of Theta Waves Reflects Place Cell Activities, and Clonidine Suppressed Firing of Place Cells in the Earlier Half of Place Fields

(A) Phase precession in asymmetric theta (AI < −0.5, left) and symmetric theta (AI > −0.5, right) in saline. Histograms represent the number of spikes in position in place field versus theta phase. Hot color means higher number of spikes.

(B) Same as (A) in clonidine.

(C) Firing rate of place cells in place field between saline and clonidine. Firing rate of place cells is calculated by using spikes fired in asymmetric theta (left) and in symmetric theta (right). Horizontal black line shows a significant difference between saline and clonidine. Mean ± SE. p < 0.05, simple main effect.
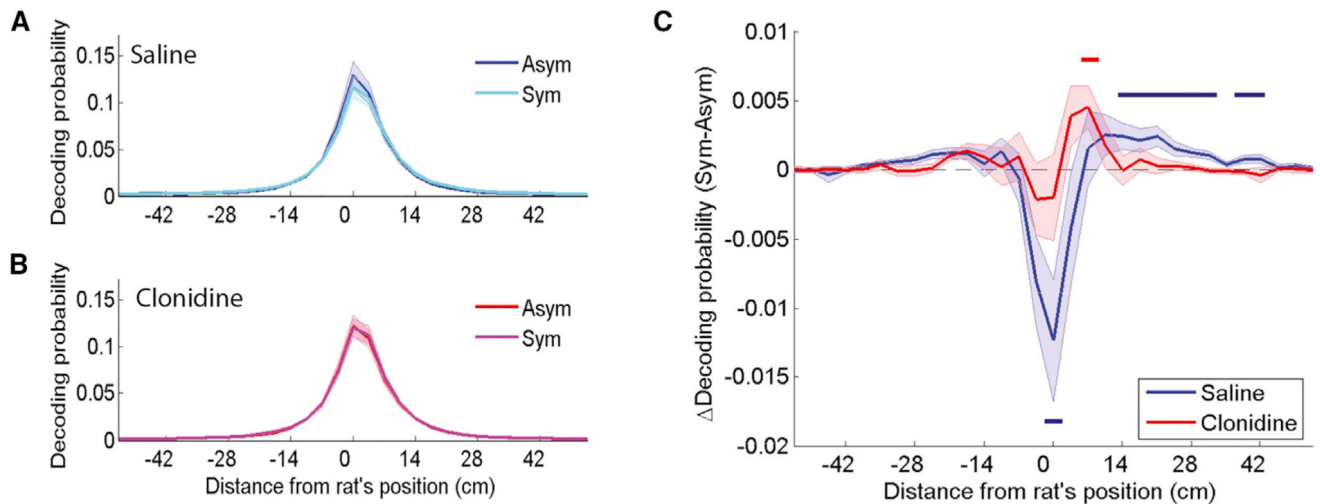
Figure 5. Theta Asymmetry Predicts Spatial Representation of Place Cells, and Clonidine Interferes with the Spatial Representation

(A) Distribution of decoding probability as spatial representation of activities of place cells' ensemble in theta cycles in saline. 0 cm on x axis shows rats' current position. Blue line shows decoding probability in asymmetric theta cycles (AI < −0.5). Light blue line shows decoding probability in symmetric theta cycles (AI > −0.5). Mean ± SE (n = 13 sessions).

(B) Same as (A) in clonidine. Red line shows decoding probability in asymmetric theta cycles. Pink line shows decoding probability in symmetric theta cycles. Mean ± SE (n = 14 sessions).

(C) Difference of spatial decoding probability between asymmetric theta and symmetric theta. 0 cm on x axis shows rats' current position. Positive value means decoding probability is higher in symmetric theta than in asymmetric theta. Negative value means decoding probability is higher in asymmetric theta than in symmetric theta. Horizontal colored lines (blue line is saline and red color in clonidine) show significant differences from 0. Mean ±SE. p<0.05, signed-rank test, two sided.